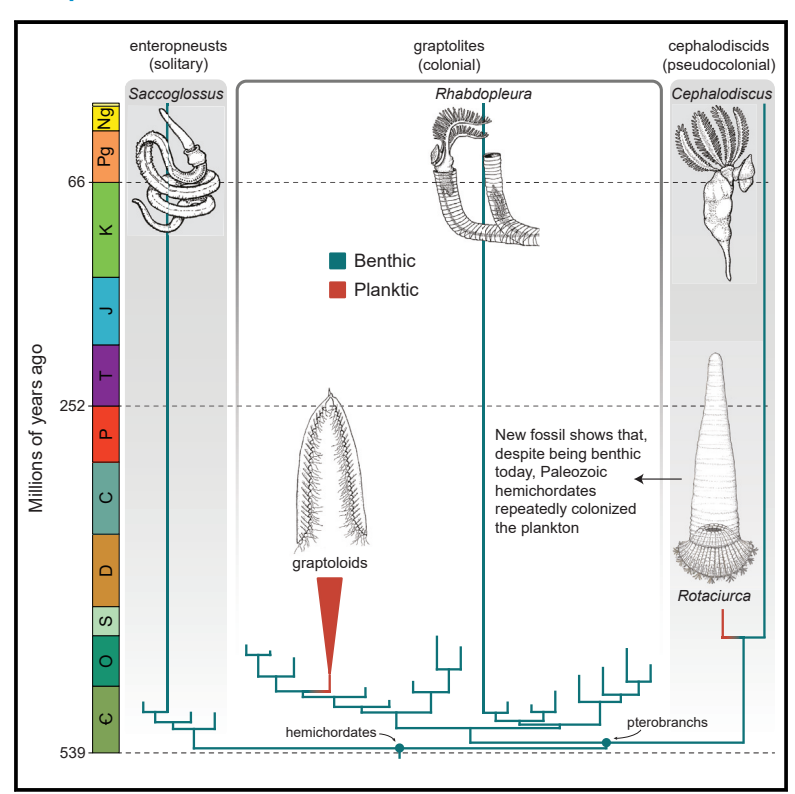
A Silurian pseudocolonial pterobranch

Graphical abstract



Authors

Derek E.G. Briggs, Nicolás Mongiardino Koch

Correspondence

derek.briggs@yale.edu (D.E.G.B.), nmongiardinokoch@ucsd.edu (N.M.K.)

In brief

Briggs and Mongiardino Koch describe a problematic Silurian fossil commonly known as Ezekiel's Wheel, which consists of radiating tubes associated with a conical structure interpreted as a float. Phylogenetic analyses place this fossil with cephalodiscids, indicating that, along with the more familiar graptolites, they also invaded the plankton.

Highlights

- A problematic fossil from the Silurian Bertie Group of Ontario is a hemichordate
- Phylogenetic analysis places it with the pseudocolonial cephalodiscids
- An associated conical structure is interpreted as a float
- Thus, cephalodiscids, like graptolites, were present in the Silurian plankton







Report

A Silurian pseudocolonial pterobranch

Derek E.G. Briggs^{1,2,5,*} and Nicolás Mongiardino Koch^{3,4,*}

- ¹Department of Earth and Planetary Sciences, Yale University, New Haven, CT 06520, USA
- ²Yale Peabody Museum, New Haven, CT 06520, USA
- ³Marine Biology Research Division, Scripps Institution of Oceanography, UC San Diego, 9500 Gilman Drive #0202, La Jolla, CA 92093, USA
- ⁴X (formerly Twitter): @phyloprog
- ⁵Lead contact
- *Correspondence: derek.briggs@yale.edu (D.E.G.B.), nmongiardinokoch@ucsd.edu (N.M.K.) https://doi.org/10.1016/j.cub.2023.10.024

SUMMARY

Pterobranchs, a major group of the phylum Hemichordata, first appear in the fossil record during the Cambrian, 1 and there are more than 600 fossil genera dominated by the mainly planktic graptolites of the Paleozoic, which are widely used as zone fossils for correlating sedimentary rock sequences.² Pterobranchs are rare today; they are sessile marine forms represented by Rhabdopleura, which is considered the only living graptolite, and Cephalodiscus. Unlike their sister taxon, the colonial graptolites, cephalodiscids are pseudocolonial.^{3,4} Here, we describe a problematic fossil from the Silurian (Pridoli) Bertie Group of Ontario (420 mya), a sequence of near-shore sediments well known for its remarkably preserved diversity of eurypterids (sea scorpions). The fossil, Rotaciurca superbus, a new genus and species, was familiarly known as Ezekiel's Wheel, with reference to the unusual circular arrangement of the tubes that compose it. The structure and arrangement of the tubes identify Rotaciurca as a pterobranch, and phylogenetic analysis groups it with the cephalodiscids. We place it in a new family Rotaciurcidae to distinguish it from Cephalodiscidae. A large structure associated with the tubes is interpreted as a float, which would distinguish Rotaciurca as the only known planktic cephalodiscid—thus cephalodiscids, like the graptolites, invaded the water column. This mode of life reflects the rarity of pseudocolonial macroinvertebrates in planktic ocean communities, a role occupied by the tunicates (Chordata) known as salps today. Our estimates of divergence times, the first using relaxed total-evidence clocks, date the origins of both hemichordates and pterobranchs to the earliest Cambrian (Fortunian).

RESULTS

Pterobranchs have a more significant fossil record than the other major group of hemichordates, enteropneusts (acorn worms), owing to their decay-resistant fusellum, ^{1,6} although some Cambrian enteropneusts secreted a tube-like structure. ^{7–9} Molecular phylogenies indicate a sister group relationship between pterobranchs and enteropneusts, ^{10–12} as do morphological data, ¹³ although earlier molecular studies found pterobranchs within enteropneusts. ^{14,15} Both orders of pterobranchs, Graptolithina and Cephalodiscida, are characterized by a tubarium of collagenous/proteinaceous tubes that accommodates zooids with tentaculated arms used in suspension feeding. ^{3,14} Graptolites invaded the water column early in the Ordovician (the earliest planktic genus is *Rhabdinopora*) ¹⁶ and are diverse and abundant through to the Lower Devonian. ² All known extant and fossil cephalodiscids are benthic. ⁴

The name of the new genus and species, *Rotaciurca superbus*, is derived from *rota* (Latin for wheel), combined with Ciurca (masculine) in honor of Samuel J. Ciurca, Jr., who donated the specimens together with thousands of eurypterids to the Yale Peabody Museum (YPM). ^{17,18} Ciurca's name for the fossil, Ezekiel's Wheel, alludes to the prophet's vision of the divine warrior riding in a wheeled chariot, as described in the Book of Ezekiel in the Bible. ¹⁹ The species name *superbus* (Latin for

excellent, superior, and splendid) acknowledges that Ciurca labeled the holotype "the most beautiful fossil ever found." We assign *R. superbus* to a new family Rotaciurcidae of the order Cephalodiscida.

Material

The ten known specimens from the late Silurian (Pridoli) Bertie Group (Bed A of the Williamsville Formation) in Ridgemount Quarry South, Fort Erie, Welland County, Ontario, Canada are registered in the Invertebrate Paleontology Division of the YPM (YPM IP). Ciurca collected the holotype (YPM IP 428141 part and counterpart; Figures 1A, 1B, and 1G–1I) in 1995 and eight other specimens over the next 25 years: YPM IP 227590 (Figures 2F and 2G), 237272 (Figures 2D and 2E), 251592 (with counterpart) (Figures 2H and 2I), 254553 (Figures 1C and 1D), 309898, 428830 (with counterpart) (Figures 2A–2C), 546797 (with counterpart) (Figures 1E and 1F). An additional specimen, YPM IP 542614 (with counterpart), was discovered by Wayne Davey and subsequently acquired by Ciurca.

Preservation

The specimens consist of a circular aggregate of radiating tubes, arranged in two or more levels, making up the tubarium. They have undergone some collapse and flattening, but the tubarium





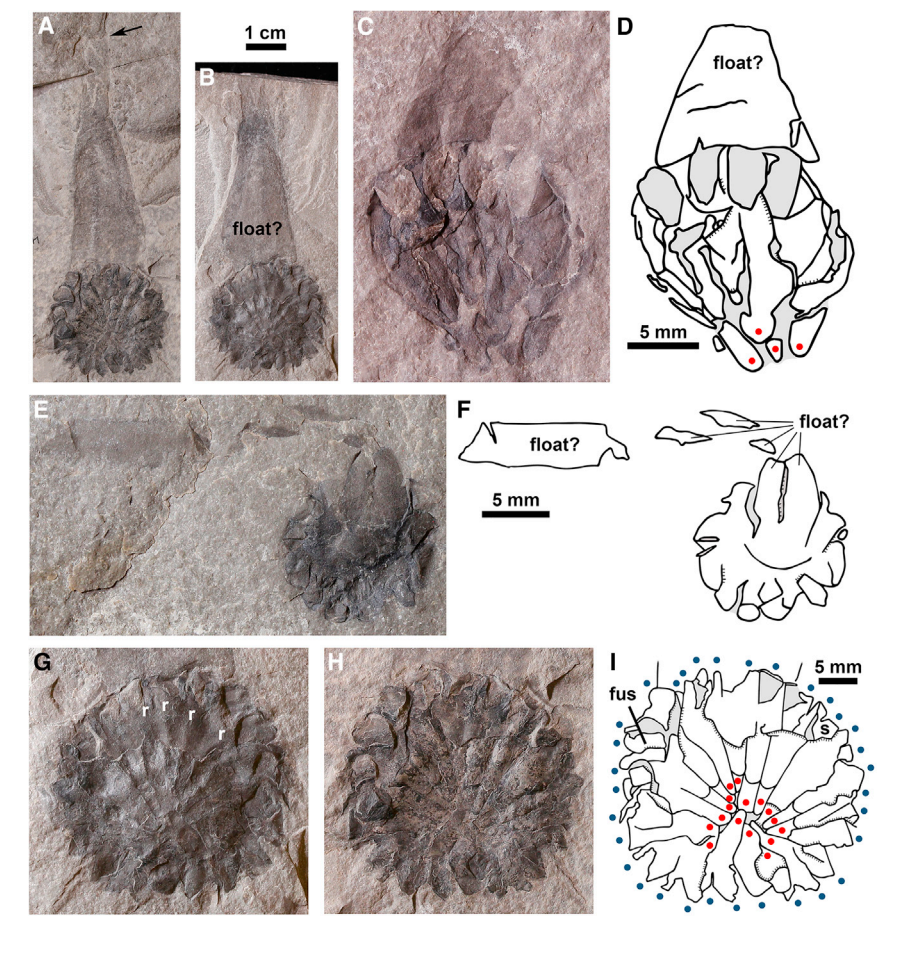


Figure 1. Rotaciurca superbus specimens showing evidence of float and arrangement of tubes

(A and B) YPM IP 428141 holotype, part, and counterpart.

(C and D) YPM IP 254553, specimen and explanatory drawing.

(E and F) YPM IP 546798, part, specimen, and explanatory drawing.

(G-I) YPM IP 428141 holotype, counterpart, part, and explanatory drawing of tubarium.

The arrow marks the preserved termination of the float. Red dots mark the origins (closed ends) of tubes, where evident on part or counterpart, blue dots represent the termination of tubes. r indicates ridges. fus shows the position of fuselli illustrated in Figure 3A. s indicates position of sample for energy dispersive X-ray spectrometer (EDS) analysis. Hachures in these and other drawings indicate pronounced changes in the level of splitting resulting in breaks of slope, the solid line at the upper edge of the break, the hachures directed downslope. See also Figure S1.

The tube walls are dark in color (Figures \$2G-\$2I) and often cracked into irregular fragments such that tubarium tissue is lost on splitting of the slabs (Figures 3E and 3F). Their organic composition is confirmed by Raman analysis that yields a set of signals associated with insoluble kerogen (C=C, C-C, C-N, C=O vibrations, aromatic rings) (Figure \$2F). The surface of the tube wall shows linear

structures (Figure 3), which we interpret as the margins of fuselli, but there is no evidence that the internal ultrastructure of the wall is preserved. The margins of the fuselli show some relief (Figure 3A), as do those in other fossils (e.g., Mierzejewski²⁰ and Mierzejewski and Kulicki²¹). This may be exaggerated by separation along the boundaries between fuselli and by some penetration of sedimentary matrix during burial and flattening (Figures 3B, 3E, and 3F). Where the separation narrows or is absent, as evidenced by continuity of the carbonaceous tubarium tissue, the relief is likewise reduced (Figures 3C, 3D, 3F, and 3G). The high proportion of carbon in the tube walls (Figure S2A), similar to that in associated eurypterid cuticle (Figures S2B and S2F), decreases in the sediment layer separating the levels of tubes within the tubarium, and it is lowest in the matrix beyond the specimen. Where the material of the wall has flaked off or is on the counterpart, the path of the tube is lighter in color but still darker than the matrix surrounding the specimen (Figure S1B), indicating an organic residue in the sediment immediately adjacent to the tubes. The central part of the organic-rich sediment layer separating the levels of tubes contains a higher weight percent of silicon than the tubes themselves and the matrix beyond the specimen, probably reflecting early cementation of the organic-rich sediment.

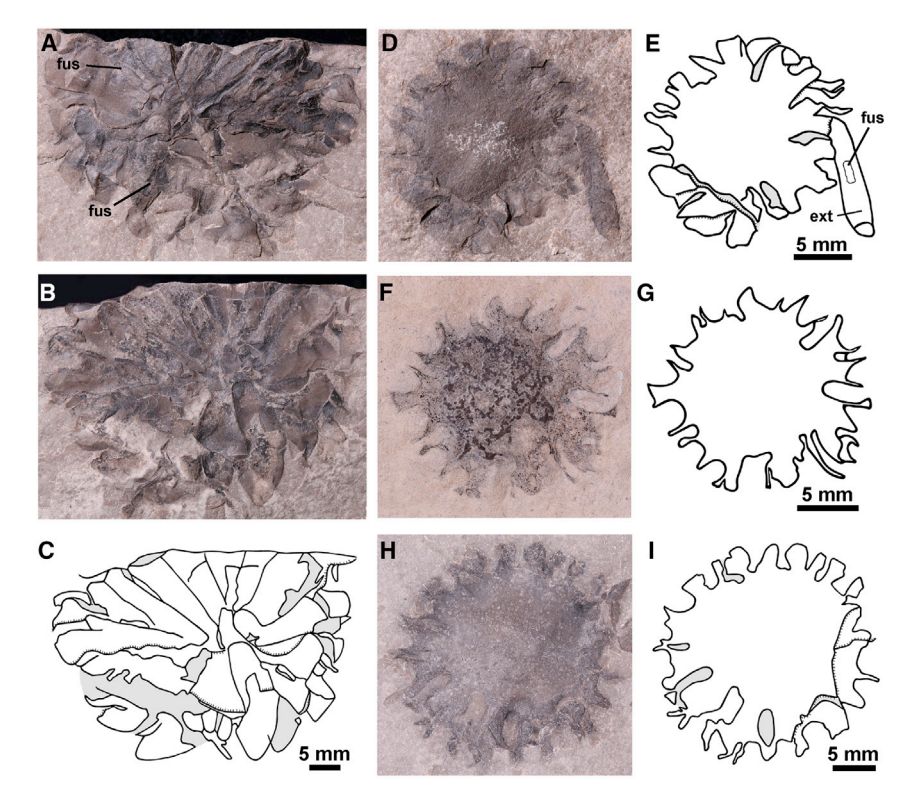
Eurypterid cuticle from this locality is composed of long-chain aliphatic components as a result of *in situ* polymerization during diagenesis.²² The similarity of the Raman spectra of the tube

is largely symmetrical in most specimens, indicating that they are preserved near parallel to bedding (Figures 1A, 1B, 2, and S1). Where the tubarium shows some asymmetry and the mid-point is not at the center (Figures 2A–2C), the specimen was tilted slightly on burial, as reflected in its attitude to the sedimentary laminations evident on the edge of the sample. A single specimen is flattened so that it affords a lateral view (Figures 1C and 1D) such that the radial arrangement of the tubes is not evident.

The holotype preserves clear evidence of two sets of radiating tubes (Figures 1G and 1H), one overlying the other, separated by a featureless organic-rich sediment layer. An essentially complete set of tubes is exposed, and a portion of the other is evident where the specimen has split along the sediment layer, separated by a break of slope. Radiating ridges on this partly exposed level (Figure 1G) do not correspond to the boundaries of the tubes that overlie it and presumably reflect the position of the tubes beneath. A different specimen (Figures 2A-2C) was broken through the periphery of the tubarium, revealing tubes in a section on the vertical break at a different level to the one exposed by splitting along the bedding plane. This confirms that the tubarium consists of two or more levels. Some specimens (e.g., Figures 2D and 2E) have split along the sediment layer that separates sets of tubes rather than at a level of tubes. Here, poorly defined ridges are the only trace of the tubes, except where they emerge at the margin of the specimens.

Report





walls and eurypterid cuticle (Figure S2F) shows that the two samples have undergone similar diagenetic alteration—arthropod cuticles and graptolite tubarium tissue behave similarly during fossilization. ^{23,24} The color of a large conical projection (Figures 1A and 1B), which preserves some relief, likewise indicates an organic residue, and in places, tiny fragments of its outer wall remain (Figure S2I). This structure is only evident in three of the ten specimens (Figure 1), indicating that it normally separated from the tubarium and/or decayed. In one case, it has flexed through ~90° (Figures 1E and 1F), presumably during transport and burial. The specimens preserve no evidence of zooids, but this is the norm among fossil pterobranchs²⁵ owing to the susceptibility of zooids to decay. ^{26,27}

Diagnoses

Phylogenetic analysis indicates that the affinities of *Rotaciurca* lie with the cephalodiscid pterobranchs, but the structure and arrangement of tubes in the new taxon differ significantly from those in any known pterobranch including order Cephalodiscida, family Cephalodiscidae.

Family Rotaciurcidae. Diagnosis as for genus and species.

Genus and species *Rotaciurca superbus*. Circular tubarium comprising two or more levels each of $\sim \! 16$ radiating organic tubes. The tubes, which have a closed convex origin and are unconnected, widen and subdivide into two (or perhaps more) branches distally. The tube walls are made up of irregular fuselli. The tubarium is attached to a conical structure (possible float).

Description

The tubarium of *Rotaciurca superbus* consists of a circular array of radiating tubular units (Figures 1, 2, and S1). The

Figure 2. *Rotaciurca superbus* specimens showing arrangement of tubes

(A–C) YPM IP 428830, part, counterpart, and explanatory drawing. Upper **fus** shows the position of fuselli illustrated in Figure 3C and lower **fus** those in Figure 3B.

(D and E) YPM IP 237272, specimen and explanatory drawing. Tubes in the bottom left overlie the organic-rich layer that separates the two layers of tubes. **ext** is the tube extension; **fus** shows the position of fuselli illustrated in Figures 3D and 3E. (F and G) YPM IP 227590, specimen and explanatory drawing.

(H and I) YPM IP 251592, specimen and explanatory drawing.

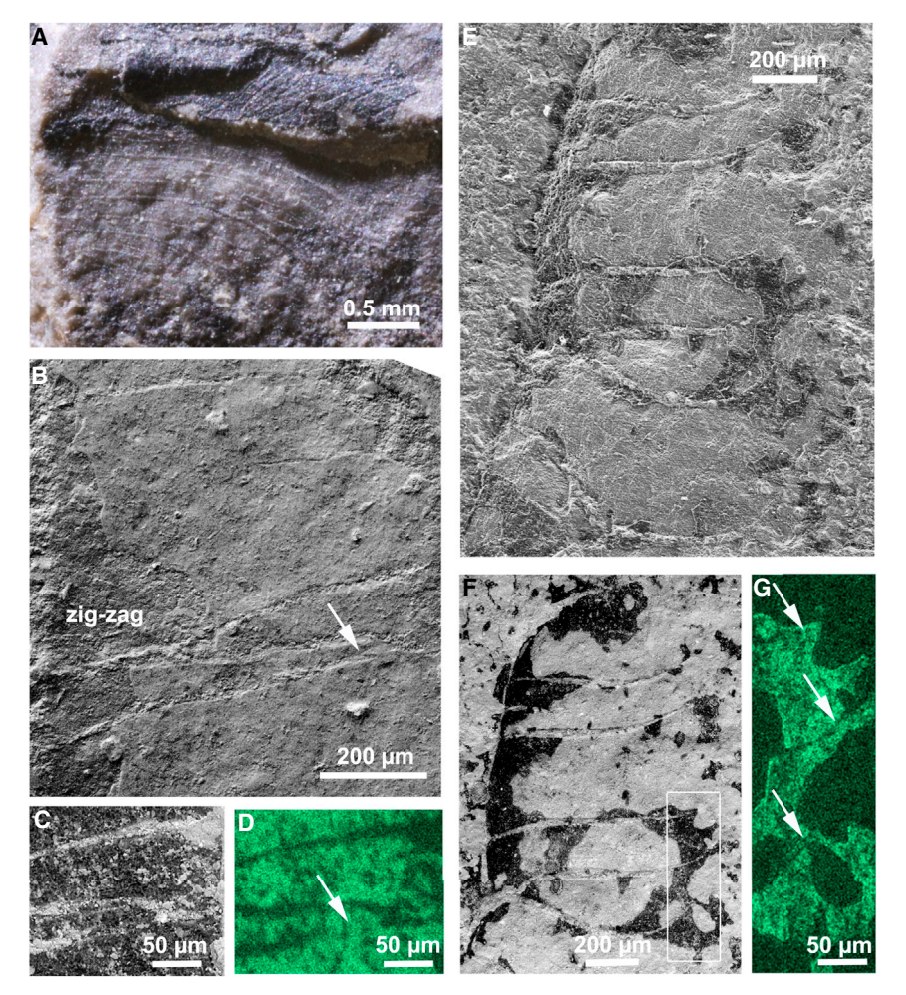
See also Figure S1.

tubarium tapers in lateral view toward the origin of the tubes at its center (Figures 1C and 1D). Its maximum preserved diameter in the known specimens ranges from 11 (Figures 1E and 1F) to 38 mm (Figure S1): mean 24.1 mm, SD 7.83 (as a population). The preserved length of the tubes ranges up to 20 mm (Figure S1). The smaller tubaria may be incomplete or may represent earlier developmental stages. It is difficult to

measure the width of the tubes at the perimeter of the tubarium because of the overlap and the way the specimens split, but it varies from \sim 2 mm in the smallest specimen to 3.5–4 mm in the larger ones. An elongate conical feature, interpreted as an attachment or float, is associated with the tubarium of YPM IP 428141 (Figures 1A and 1B). It lacks the dark layer of organic material that defines the tubes, but tiny organic fragments are evident in places on the surface indicating that a thinner wall was originally present. Two darker lines that run along the length of this feature subparallel to the margins are marked by a residue of the organic wall. They show very slight relief and appear to be a result of compaction and splitting of the specimen. Spaced transverse wrinkles may be similar in origin. The preserved length of this feature is about 2.0x the preserved diameter of the tubarium (Figures 1A and 1B) and its maximum width about 60% of the diameter, and it tapers away from its attachment to the tubarium. The maximum width of this feature in YPM IP 254553, which affords a lateral view, is about 75% that of the tubarium, and wrinkling normal to its long axis indicates shortening during flattening (Figures 1C and 1D). These differences in the relative proportions of the conical feature and tubarium reflect the contrast between preservation parallel (where the tubes are splayed outward) versus lateral to the bedding. A third example of this feature (Figures 1E and 1F) extends a short distance before flexing through $\sim 90^{\circ}$ —its total length is about 2.7× the diameter of the tubarium. In this specimen, the opposing walls are separated by a sediment fill.

The tubes radiate from the mid-point of the tubarium (Figures 1G-1I). The outline of $\sim \! 16$ closed rounded ends is evident where they are set apart (Figures 1C, 1D, and S1). In other cases, they are juxtaposed (Figures 1G-1I) or overlapping





(Figures 2A–2C). The tubes expand and divide along their length, resulting in a total of up to 32 tube openings in each level at the preserved perimeter (Figures 1G–1I and S1). This estimate is approximate due to overlap and flattening during fossilization (Figures 2A–2C). The nature and position of branching are difficult to discern. Transverse curved lines appear to indicate where the tubes divide (Figures 1G–1I); circular or arc-shaped structures along the length of some of the tubes (Figure S1) may likewise represent branching points. The opening of each tube is near straight to somewhat convex. Some of the tubes curve slightly to one side along their length, resulting in a termination outline approximating an inverted V (Figures 1G–1I).

Where specimens preserve the tube wall, it shows lineations with some relief, oriented approximately orthogonal to the axis of the tube (Figure 3). These lineations are evident on all specimens where fragments of the tube wall remain. The lineations are generally curved and subparallel, and sometimes appear discontinuous. They are separated by distances (measured parallel to the axis of the tube) from ${\sim}200$ to $400~\mu m$. The lineations occasionally show junctions that appear to zigzag (Figure 3B) and are sometimes irregular. They are interpreted as the margins of fuselli.

A number of smaller specimens are characterized by fewer tube openings, often concave outward, at the perimeter: \sim 16

Figure 3. Rotaciurca superbus, details of tube wall showing fuselli

(A) YPM IP 428141 part, low angle light (see Figure 1I).

(B–D) YPM IP 428830 (see Figure 2A). (B) Back-scatter SEM showing zigzag, (C) backscatter SEM showing fusellar boundaries, and (D) EDS carbon map.

(E–G) YPM IP 237272, area on tube extension (see Figure 2E). (E) Secondary electron SEM, (F) backscatter SEM of upper part of area in (E), and (G) EDS carbon map of area indicated in (F). Arrows indicate where separation of fusellar tissue and intrusion of sediment are minimal.

See also Figure S2.

(Figures 2F and 2G) to ~20 (Figures 2H and 2I). In these cases (Figures 2D-2I), the tubes themselves are largely concealed by organic-rich sediment. One specimen is unusual in preserving an apparent extension of one of the tubes (Figures 2D and 2E), which curves through an angle where it projects from the tubarium, its thickness reflected in a break of slope. The lateral margins of this possible extension appear to be contiguous with a tube within the "wheel." The extension is similar in width to the associated tube expanding just a little distally, and it is dark in color like the rest of the specimen. The surface is wrinkled, suggesting that the fusellum is thinner, but a patch of the wall shows fuselli running roughly normal to

the tube axis (Figures 3E and 3F). Where the extension bends, faint traces of fuselli are evident both above and below the break of slope (i.e., on both sides of its attachment to the "wheel"), and here, they are likewise normal to the tube axis. It is possible that this specimen, and others like it, represent only the central part of the tubarium, corresponding to the area partly delimited by curved lines traversing the tubes, perhaps branching points, in YPM IP 428141 (Figures 1H and 1I) and YPM IP 546797 (Figure S1)—the dimensions are compatible. Alternatively, the extension may represent a tube displaced from the center of the tubarium, but its length exceeds that of preserved radius, making this unlikely. Thus, the outer part of the tubes may have been lost in some specimens due to separation and/or decay.

DISCUSSION

Affinities

The affinities of *Rotaciurca superbus* have been a mystery since its discovery. The first image in the scientific literature was published in 2008 by Nudds and Selden,⁵ who confessed they had "no idea what this organism is" but suggested it was most likely part of a plant like *Cooksonia*, which also occurs in the Bertie Group.²⁸ Our results show that *R. superbus* is an aggregate of tubes with organic walls showing lineations that demarcate

Report



fuselli, a synapomorphic character of pterobranchs.^{3,29} The arrangement of fuselli is less regular than in other pterobranchs, but these features do not lend themselves to an alternative interpretation. Other taxa have been identified as pterobranchs based on a similar suite of attributes. 30-32 Fossils of Yuknessia, for example, from the Trilobite Beds on Mount Stephen, British Columbia and other Cambrian localities, which are also composed of carbon, were long interpreted as an alga until a combination of fine details and overall morphology revealed a pterobranch affinity.30 Y. stephenensis, the larger more completely known species, shares a number of similarities with R. superbus. The tubes are rigid and lack folding or wrinkling. Details of the central area of the tubarium, like those in R. superbus, are often concealed by overlapping tubes, and evidence of branching is difficult to discern. The tubes in Y. stephenensis range up to 20 mm in length, similar to their maximum preserved length in R. superbus, but they are narrower (from 0.1 at the base to 1 mm at the aperture) than those in R. superbus that are up to 4 mm wide at the aperture. Apart from the morphology of the tubarium, a key feature in determining a pterobranch affinity of Y. stephenensis was the presence of fusellar banding. The mean height of the fuselli in Y. stephenensis is 0.032 mm, whereas those in R. superbus are less regularly spaced and 0.2-0.4 mm in height, perhaps reflecting the difference in the width of the tubes. The boundaries between fuselli show relief in both cases, and neither displays a consistent zigzag pattern or evidence of a stolon. A relationship between the dimensions of fuselli and zooid size has been detected in Rhabdopleura and inferred in graptolites, 33 but see Maletz. 34 However, variation in the relationship between tube width and fusellar height has been noted in fossil *Rhabdopleura*³⁵ and even in individual Rhabdopleura obuti,36 for example.

The arrangement of fuselli in R. superbus is irregular, compared with that in most graptolites, even in Cambrian forms such as Rhapdopleura obuti from Cambrian Series 3 of Siberia.36-39 a taxon recently assigned to Graptolithina incertae sedis. 40 Fuselli are less regular in cephalodiscids. 41 The irregular fuselli of R. superbus and lack of connections between tubes where they originate at the center of the tubarium contrast with the morphology of graptolites and are reminiscent of the pseudocolonial organization found among cephalodiscids.^{29,47}

Other colonial animals with an outer organic skeleton, such as hydroids⁴³ and bryozoans, might be confused with pterobranchs. Hydroids, however, form networks of thecae that branch irregularly from a stolon or regularly at the stolon terminus, 44 patterns that differ from that in R. superbus where the thecae are not connected at their origin. Similar considerations apply to bryozoans that lack a calcified skeleton-neither the colony form nor branching structure⁴⁵ resembles that in R. superbus. Structures resembling fuselli are not present in the outer skeleton of hydroids or bryozoans.

Our analysis of the phylogenetic position of R. superbus is based on the characters (Data S1 and S2) listed by Ramírez-Guerrero and Cameron,31 which were in turn based largely on those used in a previous investigation of graptolite phylogeny.²⁹ These are complemented with mitochondrial genome⁴⁶ and 18S rDNA⁴⁷ information for all main clades of living hemichordates, used to further inform their divergence times. Parsimony and undated Bayesian analyses of morphology provide weak support for placing R. superbus as sister to crown-group pterobranchs (Figures S3A and S3B). Time-calibrated (tip-dated) analyses of both morphological and total-evidence datasets (Figures S3C-S3F) favor a less resolved consensus (especially among graptolites) instead of unwarranted levels of resolution.⁴⁸ The results, however, strongly support a cephalodiscid relationship for R. superbus. We adopt this more conservative result and place R. superbus in a new family Rotaciurcidae, to distinguish it from family Cephalodiscidae, within the order Cephalodiscida.

Total-evidence dating resulted in narrower confidence intervals for divergence times and younger median estimates, compared with those based on morphology alone, a result that recapitulates recent simulations. 49 Pterobranchs and enteropneusts diverged in the early Cambrian (Fortunian), approximately 10 Ma younger than previous estimates. 11 Cephalodiscids and graptolites (i.e., crown-group Pterobranchia, a node so far lacking divergence time estimates) split shortly (<5 Ma) thereafter, consistent with the earliest known pterobranch fragments from the Fortunian of Ukraine. 6 Rotaciurca is confidently placed outside the clade of extant Cephalodiscus, which is inferred to have originated in the Triassic (although dates are poorly constrained). Assigning this fossil to the cephalodiscid stem group, however, is complicated by the uncertain affinities of the extant genus Atubaria²⁹—in the absence of clear evidence for the relationship between this unusual living taxon and fossil members of the clade, the distinction between stem and crown groups cannot be delineated with confidence. Regardless, Rotaciurca increases the known morphological disparity of cephalodiscids and extends the depauperate Paleozoic record of the clade beyond Cambrian and Ordovician strata. 1 Rotaciurca also stands out as the only planktic cephalodiscid, if our interpretation of its ecology is correct, indicating cephalodiscids, just like graptolites, colonized the plankton (Figure S4).

Paleoecology

There is a risk that, depending on rates of sedimentation, the zooids of Rotaciurca superbus would have been buried if it were benthic, unless the pseudocolony was elevated above the seafloor. The conical feature that is preserved in some specimens (Figures 1 and 4) might have functioned in attachment to the substrate or support above it, but if so, a robust structure would be expected. However, this feature lacks the thicker organic wall of the tubes, as evidenced by its different preservation (Figures S2G and S2I). An alternative interpretation is that it represents a float, and the orientation of specimens in our figures shows this possibility. The circular shape and symmetry of the tubarium of R. superbus are not at odds with a planktic mode of life, 16,42 but some benthic graptolites, such as Sphenoecium, may show a similar radiating arrangement of tubes (Maletz⁵⁰; Figure 1A, Museum of Comparative Zoology.IP.199806, scale is 1 cm not 1 mm). The float may have promoted rotation in the water column because of current flow, which has been shown to increase the efficiency of feeding in graptolites.⁵¹

Previously known cephalodiscids are benthic, but a variety of possible floats (nematularia) evolved in different graptolites;^{34,40} as in this case, however, they are rarely preserved. 52,53 Nematularia are associated with the nema, but a possible float of different origin is known in the early planktic graptolite Rhabdinopora proparabola. 6,16 The origin and development of the nema are



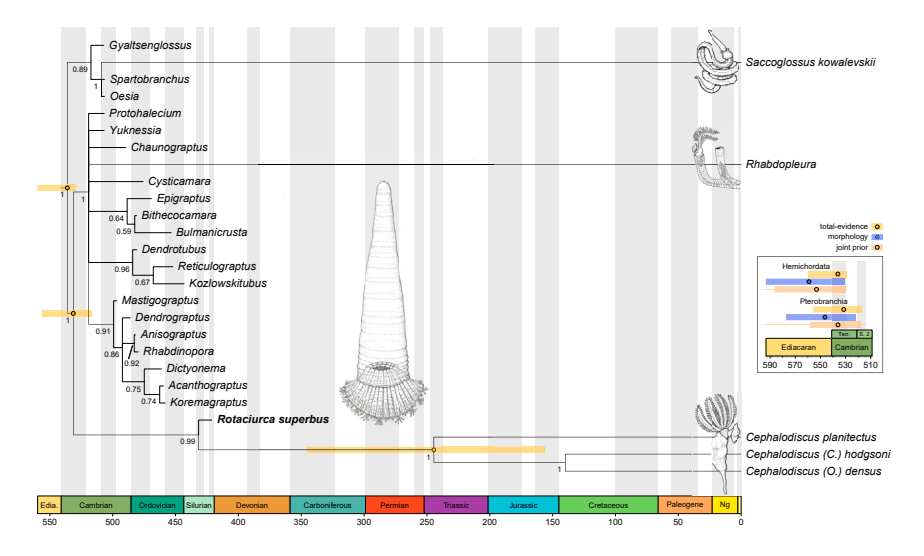


Figure 4. Phylogeny of Rotaciurca superbus and related taxa

Total-evidence dated phylogeny inferred under a skyline fossilized birth-death (FBD) model incorporating a reconstruction of Rotaciurca superbus. Tree topology corresponds to the 50% majorityrule consensus tree. Numbers represent node posterior probabilities. Dates for crown nodes were inferred with and without molecular data and are summarized using median values and 95% highest posterior density intervals, shown as circles and bars, respectively, on the inset on the right. A morphological clock dates Hemichordata to 559.1 Ma (530.9-593.4 Ma) and Pterobranchia to 546.4 Ma (522.0-577.3 Ma). Total-evidence clocks support younger ages, dating Hemichordata to 536.1 Ma (529.0-559.8 Ma) and Pterobranchia to 531.4 Ma (517.0-555.8 Ma).

See also Figures S3 and S4, Tables S1 and S2, and Data S1 and S2.

uncertain, and there is no equivalent structure in cephalodiscids. The specimens of R. superbus provide no evidence of the origin of the conical structure apart from the presence of an apparently thin decay-prone organic outer surface, which may have been constructed by the zooids. The possibility that the conical structure functioned as a float raises the question of how R. superbus would have maintained its position in the water column. There are no planktic pterobranchs today to provide observational data. It is not known whether graptolites achieved neutral buoyancy⁵⁴ or relied on a combination of factors, including drag and/or propulsion, to move in the water column, R. superbus is relatively large, but strategies for inhabiting the water column presumably functioned in proportion to the size and weight of the colony. The large tubes in R. superbus would have accommodated larger zooids than those in graptolites. If it were planktic, it is likely that R. superbus was capable of some form of active locomotion. but the only feasible mode would have involved the zooids, 55 and there is no evidence available to assess that.

The dolomites of the Bertie Group are interpreted as shallow restricted marine sediments that formed where there was significant evaporation.⁵ There is some debate, however, about the salinity of the water where the fossils are preserved, and conditions may not have been hypersaline.⁵⁶ Nonetheless benthic animals are rare in the unit that yields R. superbus and are confined to small gastropods and brachiopods that represent less than 2% of specimens from Bed A in Ridgemount Quarry South in the YPM Ciurca collection, excluding the benthic alga Inocladus Iesquereuxi⁵⁷ and the plant Cooksonia,²⁸ which was washed in from the land. Eurypterids are the main faunal element, but they are represented exclusively by exuviae, and there is a consensus that their normal habitat was elsewhere-they congregated and molted in this setting. Nautiloids, mainly straight but also coiled, are present and were likewise swimmers. A single largely complete acanthodian has also been recovered.⁵⁸ R. superbus is known only from this locality, which is an unusually limited distribution for a planktic form, but the exceptional conditions may have been essential to its preservation. Thus, the evidence of the associated biota is consistent with an interpretation of *R. superbus* as planktic.

The organization of *R. superbus* as a pseudocolony is different from other planktic pterobranchs, i.e., graptolites, where individual zooids are connected by a stolon. Pseudocolonial macroinvertebrates are represented in the plankton today by salps. ^{59,60} If our interpretation of *R. superbus* as planktic is correct, it expands the taxonomic and temporal breadth of this unusual ecological strategy.

STAR*METHODS

Detailed methods are provided in the online version of this paper and include the following:

- KEY RESOURCES TABLE
- RESOURCE AVAILABILITY
 - Lead contact
 - Materials availability
 - Data and code availability
- EXPERIMENTAL MODEL AND SUBJECT DETAILS
- METHOD DETAILS
 - Imaging and chemical analyses
- QUANTIFICATION AND STATISTICAL ANALYSIS
 - Phylogenetic analyses
 - Ancestral state reconstructions

SUPPLEMENTAL INFORMATION

Supplemental information can be found online at https://doi.org/10.1016/j.cub.2023.10.024.

ACKNOWLEDGMENTS

We are grateful to Susan Butts and Jessica Utrup (Yale Peabody Museum) for collections support. J. Utrup identified a number of specimens while unpacking material from the Ciurca bequest. She took the photographs, and Zhenting Jiang assisted with scanning electron microscopy and EDS analysis. Brian Roach drew the reconstruction of *Rotaciurca* and the line drawings of living organisms. Yuanning Li provided the sequences of the mitochondrial loci. Jennifer Girard and Jasmina Wiemann assisted in obtaining and processing Raman spectra. We are grateful to Steven LoDuca and two anonymous reviewers for detailed comments that helped us in preparing the final version.

Report

CellPress

N.M.K. was supported by National Science Foundation grant DEB-2036186 (awarded to Grea W. Rouse).

AUTHOR CONTRIBUTIONS

Conceptualization, D.E.G.B.; methodology, D.E.G.B. and N.M.K.; investigation, D.E.G.B. and N.M.K.; writing - original draft, D.E.G.B. based on a graduate class project by N.M.K.; writing - review & editing, D.E.G.B. and N.M.K.

DECLARATION OF INTERESTS

D.E.G.B. is a member of the Advisory Board of Current Biology.

Received: May 2, 2023 Revised: July 7, 2023 Accepted: October 16, 2023

Published: November 6, 2023; corrected online: November 14, 2023

REFERENCES

- 1. Maletz, J. (2014). Hemichordata (Pterobranchia, Enteropneusta) and the fossil record. Palaeogeogr. Palaeoclimatol. Palaeoecol. 398, 16-27.
- 2. Zalasiewicz, J.A., Taylor, L., Rushton, A.W.A., Loydell, D.K., Rickards, R.B., and Williams, M. (2009). Graptolites in British stratigraphy. Geol. Mag. 146, 785-850.
- 3. Maletz, J. (2014). The classification of the Pterobranchia (Cephalodiscida and Graptolithina). Bull. Geosci. 89, 477-540.
- 4. Maletz, J., and Gonzalez, P. (2017). Order Cephalodiscida: introduction and systematic descriptions. Chapter 14. In Treatise Online, Second Revision. Part V, 100, pp. 1-8.
- 5. Nudds, J.R., and Selden, P.A. (2008). Fossil Ecosystems of North America (University of Chicago Press), p. 288.
- 6. Maletz, J. (2019). Tracing the evolutionary origins of the Hemichordata (Enteropneusta and Pterobranchia). Palaeoworld 28, 58-72.
- 7. Nanglu, K., Caron, J.B., Conway Morris, S., and Cameron, C.B. (2016). Cambrian suspension-feeding tubicolous hemichordates. BMC Biol.
- 8. Nanglu, K., Caron, J.B., and Cameron, C.B. (2020). Cambrian tentaculate worms and the origin of the hemichordate body plan. Curr. Biol. 30, 4238-4244.e1.
- 9. Caron, J.B., Morris, S.C., and Cameron, C.B. (2013). Tubicolous enteropneusts from the Cambrian period. Nature 495, 503-506.
- 10. Cannon, J.T., Kocot, K.M., Waits, D.S., Weese, D.A., Swalla, B.J., Santos, S.R., and Halanych, K.M. (2014). Phylogenomic resolution of the hemichordate and echinoderm clade. Curr. Biol. 24, 2827-2832.
- 11. Simakov, O., Kawashima, T., Marlétaz, F., Jenkins, J., Koyanagi, R., Mitros, T., Hisata, K., Bredeson, J., Shoguchi, E., Gyoja, F., et al. (2015). Hemichordate genomes and deuterostome origins. Nature 527, 459-465.
- 12. Tagawa, K. (2016). Hemichordate models. Curr. Opin. Genet. Dev. 39. 71-78.
- 13. Cameron, C.B. (2005). A phylogeny of the hemichordates based on morphological characters. Can. J. Zool. 83, 196-215.
- 14. Cameron, C.B., Garey, J.R., and Swalla, B.J. (2000). Evolution of the chordate body plan: new insights from phylogenetic analyses of deuterostome phyla. Proc. Natl. Acad. Sci. USA 97, 4469-4474.
- 15. Cannon, J.T., Rychel, A.L., Eccleston, H., Halanych, K.M., and Swalla, B.J. (2009). Molecular phylogeny of Hemichordata, with updated status of deep-sea enteropneusts. Mol. Phylogenet. Evol. 52, 17-24.
- 16. Maletz, J. (2017). The planktic revolution. Chapter 9. In Graptolite Paleobiology, J. Maletz, ed. (Wiley Blackwell), pp. 139-152.
- 17. Brett, C.E. (2017). Presentation of the 2016 Harrell L. Strimple Award of the Paleontological Society to Samuel J. Ciurca, Jr. J. Paleontol. 91, 1356-1357.

- 18. Briggs, D.E.G., and Roach, B.T. (2020). Excavating eurypterids, giant arthropods of the Palaeozoic. Geol. Today 36, 16-21.
- 19. Ciurca, S.J., Jr. (2008). Mystery fossil Ezekiel's wheel. Priscum. Newsletter of the Paleontological Society 14, 1-22.
- 20. Mierzejewski, P. (1984). Pterobranchites Kozlowski 1967 an aberrant graptolite? Acta Palaeontol. Pol. 29, 83-89.
- 21. Mierzejewski, P., and Kulicki, C. (2001). Graptolite-like fibril pattern in the fusellar tissue of Palaeozoic rhabdopleurid pterobranchs. Acta Palaeontol. Pol. 46, 349-366
- 22. Gupta, N.S., Tetlie, O.E., Briggs, D.E.G., and Pancost, R.D. (2007). The fossilization of eurypterids: a result of molecular transformation. Palaios
- 23. Gupta, N.S., Briggs, D.E.G., and Pancost, R.D. (2006). Molecular taphonomy of graptolites. J. Geol. Soc. Lond. 163, 897-900.
- 24. Maletz, J. (2020). Hemichordata (Enteropneusta & Pterobranchia, incl. Graptolithina): a review of their fossil preservation as organic material. Bull. Geosci. 95, 41-80.
- 25. Maletz, J., and Cameron, C.B. (2016). Introduction to the Class Pterobranchia Lankester, 1877. Chapter 3. In Treatise Online, Second Revision, Part V, 82, pp. 1-15.
- 26. Briggs, D.E.G., Kear, A.J., Baas, M., de Leeuw, J.W., and Rigby, S. (1995). Decay and composition of the hemichordate Rhabdopleura: implications for the taphonomy of graptolites. Lethaia 28, 15-23.
- 27. Beli, E., Piraino, S., and Cameron, C.B. (2017). Fossilization processes of graptolites: insights from the experimental decay of Rhabdopleura sp. (Pterobranchia). Palaeontology 60, 389-400.
- 28. Edwards, D., Banks, H.P., Ciurca, S.J., Jr., and Laub, R.S. (2004). New Silurian cooksonias from dolostones of north-eastern North America. Bot. J. Linn. Soc. 146, 399-413.
- 29. Mitchell, C.E., Melchin, M.J., Cameron, C.B., and Maletz, J. (2013). Phylogenetic analysis reveals that Rhabdopleura is an extant graptolite. Lethaia 46, 34-56.
- 30. LoDuca, S.T., Caron, J.-B., Schiffbauer, J.D., Xiao, S., and Kramer, A. (2015). A reexamination of Yuknessia from the Cambrian of British Columbia and Utah. J. Paleontol. 89, 82-95.
- 31. Ramírez-Guerrero, G.M., and Cameron, C.B. (2021). Systematics of pterobranchs from the Cambrian Period Burgess Shales of Canada and the early evolution of graptolites. Bull. Geosci. 96, 1-18.
- 32. Maletz, J., Steiner, M., and Fatka, O. (2005). Middle Cambrian pterobranchs and the question: what is a graptolite? Lethaia 38, 73-85.
- 33. Rigby, S., and Sudbury, M. (1995). Graptolite ontogeny and the size of the graptolite zooid. Geol. Mag. 132, 427-433.
- 34. Maletz, J. (2015). Graptolite reconstructions and interpretations. Paläontol. Z. 89, 271-286.
- 35. Kulicki, C. (1969). The discovery of Rhabdopleura (Pterobranchia) in the Jurassic of Poland. Acta Palaeontol. Pol. 14, 537-551.
- 36. Sennikov, N.V. (2016). Morphology of the exoskeleton and soft tissues of Cambrian rhabdopleurids. Paleontol. J. 50, 1626-1636.
- 37. Bengtson, S., and Urbanek, A. (1986). Rhabdotubus, a Middle Cambrian rhabdopleurid hemichordate. Lethaia 19, 293-308.
- 38. Durman, P.N., and Sennikov, N.V. (1993). A new rhabdopleurid hemichordate from the Middle Cambrian of Siberia. Palaeontology 36, 283-296.
- 39. Maletz, J., and Steiner, M. (2015). Graptolites (Hemichordata, Pterobranchia) preservation and identification in the Cambrian Series 3. Palaeontology 58, 1073-1107.
- 40. Maletz, J., and Beli, E. (2018). Subclass Graptolithina and Incertae Sedis Family Rhabdopleuridae: introduction and systematic descriptions. Chapter 15. In Treatise Online, Second Revision. Part V, 101, pp. 1-14.
- 41. Gonzalez, P., and Cameron, C.B. (2012). Ultrastructure of the coenecium of Cephalodiscus (Hemichordata: Pterobranchia). Can. J. Zool. 90,



- 42. Maletz, J., Lenz, A.C., and Bates, D.E.B. (2016). Morphology of the pterobranch tubarium. Chapter 4. In Treatise Online, Second Revision. Part V, 76. pp. 1-63.
- 43. Muscente, A.D., Allmon, W.D., and Xiao, S. (2016). The hydroid fossil record and analytical techniques for assessing the affinities of putative hydrozoans and possible hemichordates. Palaeontology 59, 71-87.
- 44. Kosevich, I.A. (2005). Branching in colonial hydroids. In Branching Morphogenesis, J.A. Davies, ed. (Springer), pp. 91-112.
- 45. Taylor, P.D., and Waeschenbach, A. (2015). Phylogeny and diversification of bryozoans. Palaeontology 58, 585-599.
- 46. Li, Y., Kocot, K.M., Tassia, M.G., Cannon, J.T., Bernt, M., and Halanych, K.M. (2019). Mitogenomics reveals a novel genetic code in Hemichordata. Genome Biol. Evol. 11, 29–40.
- 47. Miyamoto, N., Nishikawa, T., and Namikawa, H. (2020). Cephalodiscus planitectus sp. nov. (Hemichordata: Pterobranchia) from Sagami Bay, Japan, Zoolog, Sci. 37, 79-90.
- 48. Mongiardino Koch, N., Garwood, R.J., and Parry, L.A. (2021). Fossils improve phylogenetic analyses of morphological characters. Proc. Biol.
- 49. Mongiardino Koch, N., Garwood, R.J., and Parry, L.A. (2023). Inaccurate fossil placement does not compromise tip-dated divergence times. Preprint at bioRxiv. https://doi.org/10.1101/2022.08.25.505200.
- 50. Maletz, J. (2023). Graptolites survival in the Palaeozoic seas. Published online July 6, 2023. Hist. Biol. https://doi.org/10.1080/08912963.2023.
- 51. Rigby, S. (1992). Graptoloid feeding efficiency, rotation and astogeny. Lethaia 25, 51-68.
- 52. Finney, S.C. (1979). Mode of life of planktonic graptolites: flotation structure in Ordovician Dicellograptus sp. Paleobiology 5, 31-39.
- 53. Finney, S.C., and Jacobson, S.R. (1985). Flotation devices in planktic graptolites. Lethaia 18, 349-359.
- 54. Bates, D.E.B. (1987). The density of graptoloid skeletal tissue, and its implication for the volume and density of the soft tissue. Lethaia 20,
- 55. Melchin, M.J., and DeMont, M.E. (1995). Possible propulsion modes in Graptoloidea: a new model for graptoloid locomotion. Paleobiology 21,
- 56. Vrazo, M.B., Brett, C.E., and Ciurca, S.J., Jr. (2016). Buried or brined? Eurypterids and evaporites in the Silurian Appalachian basin. Palaeogeogr. Palaeoclimatol. Palaeoecol. 444, 48-59.
- 57. LoDuca, S.T., Swinehart, A.L., LeRoy, M.A., Tetreault, D.K., and Steckenfinger, S. (2021). Codium-like taxa from the Silurian of North America: morphology, taxonomy, paleoecology, and phylogenetic affinity. J. Paleontol. 95, 207-235.
- 58. Burrow, C.J., and Rudkin, D. (2014). Oldest near-complete acanthodian: the first vertebrate from the Silurian Bertie formation Konservat-Lagerstätte, Ontario. PLoS One 9, e104171.
- 59. Alldredge, A.L., and Madin, L.P. (1982). Pelagic tunicates: unique herbivores in the marine plankton. BioScience 32, 655-663.
- 60. Ringvold, H., Hatlevik, A., Hevrøy, J., Hughes, M., and Aukan, N. (2020). Encounters with the rare genus Helicosalpa (Chordata, Thaliacea, Salpida), using citizen science data. Mar. Biol. Res. 16, 369-379.
- 61. Goloboff, P.A., and Catalano, S.A. (2016). TNT version 1.5, including a full implementation of phylogenetic morphometrics. Cladistics 32, 221-238.
- 62. Ronquist, F., Teslenko, M., Van Der Mark, P., Ayres, D.L., Darling, A., Höhna, S., Larget, B., Liu, L., Suchard, M.A., and Huelsenbeck, J.P.

- (2012). MrBayes 3.2: efficient Bayesian phylogenetic inference and model choice across a large model space. Syst. Biol. 61, 539-542.
- 63. Edgar, R.C. (2004). MUSCLE: multiple sequence alignment with high accuracy and high throughput. Nucleic Acids Res. 32, 1792-1797.
- 64. Katoh, K., and Standley, D.M. (2013). MAFFT Multiple Sequence Alignment, Software version 7: improvements in performance and usability. Mol. Biol. Evol. 30, 772-780.
- 65. Minh, B.Q., Schmidt, H.A., Chernomor, O., Schrempf, D., Woodhams, M.D., von Haeseler, A., and Lanfear, R. (2020). IQ-TREE 2: new models and efficient methods for phylogenetic inference in the genomic era. Mol. Biol. Evol. 37, 1530-1534.
- 66. Bouckaert, R., Heled, J., Kühnert, D., Vaughan, T., Wu, C.H., Xie, D., Suchard, M.A., Rambaut, A., and Drummond, A.J. (2014). BEAST 2: a software platform for Bayesian evolutionary analysis. PLoS Comput. Biol. 10,
- 67. R Core Team (2022). R: A Language and Environment for Statistical Computing (R Foundation for Statistical Computing). https://www. R-project.org/.
- 68. Revell, L.J. (2012). phytools: an R package for phylogenetic comparative biology (and other things). Methods Ecol. Evol. 3, 217-223.
- 69. Li, Y., Dunn, F.S., Murdock, D.J.E., Guo, J., Rahman, I.A., and Cong, P. (2023). Cambrian stem-group ambulacrarians and the nature of the ancestral deuterostome. Curr. Biol. 33, 2359-2366.e2.
- 70. Lewis, P.O. (2001). A likelihood approach to estimating phylogeny from discrete morphological character data. Syst. Biol. 50, 913–925.
- 71. Heath, T.A., Huelsenbeck, J.P., and Stadler, T. (2014). The fossilized birthdeath process for coherent calibration of divergence-time estimates. Proc. Natl. Acad. Sci. USA 111, E2957-E2966.
- 72. WoRMS Editorial Board (2022). World Register of Marine Species (VLIZ). https://www.marinespecies.org.
- 73. Slater, B.J., Harvey, T.H.P., and Butterfield, N.J. (2018). Small carbonaceous fossils (SCFs) from the Terreneuvian (Lower Cambrian) of Baltica. Palaeontology 61, 417-439.
- 74. Erwin, D.H., Laflamme, M., Tweedt, S.M., Sperling, E.A., Pisani, D., and Peterson, K.J. (2011). The Cambrian conundrum: early divergence and later ecological success in the early history of animals. Science 334,
- 75. Zhang, C., Stadler, T., Klopfstein, S., Heath, T.A., and Ronquist, F. (2016). Total-evidence dating under the fossilized birth-death process. Syst. Biol. 65, 228-249.
- 76. Koren', T.N., and Rickards, R.B. (1979). Extinction of the graptolites. Geological Society of London, Special Publications 8, 457-466.
- 77. Maletz, J., Mottequin, B., Olive, S., Gueriau, P., Pernègre, V., Prestianni, C., and Goolaerts, S. (2020). Devonian and Carboniferous dendroid graptolites from Belgium and their significance for the taxonomy of the Dendroidea. Geobios 59, 47-59.
- 78. Kalyaanamoorthy, S., Minh, B.Q., Wong, T.K.F., von Haeseler, A., and Jermiin, L.S. (2017). ModelFinder: fast model selection for accurate phylogenetic estimates. Nat. Methods 14, 587-589.
- 79. Chernomor, O., von Haeseler, A., and Minh, B.Q. (2016). Terrace aware data structure for phylogenomic inference from supermatrices. Syst. Biol. 65, 997-1008.
- 80. Brown, J.W., and Smith, S.A. (2018). The past sure is tense: on interpreting phylogenetic divergence time estimates. Syst. Biol. 67, 340-353.
- 81. Huelsenbeck, J.P., Nielsen, R., and Bollback, J.P. (2003). Stochastic mapping of morphological characters. Syst. Biol. 52, 131-158.



STAR*METHODS

KEY RESOURCES TABLE

REAGENT or RESOURCE	SOURCE	IDENTIFIER
Biological samples		
Fossil Rotaciurca superbus	Yale Peabody Museum Invertebrate Paleontology Division	YPM IP 428141 (holotype) and 9 additional specimens (see Material for details)
Deposited data		
Data S1	Present study	Supplemental Information: Data S1
Data S2	Present study	Supplemental Information: Data S2
Table S1	Present study	Supplemental Information: Table S1
Table S2	Present study	Supplemental Information: Table S2
Software and algorithms		
Spectragryph v. 1.2	Friedrich Menges Spectroscopy Ninja	https://www.effemm2.de/spectragryph/
TNT v. 1.5	Goloboff and Catalano ⁶¹	https://www.lillo.org.ar/phylogeny/tnt/
MrBayes v. 3.2.7a	Ronquist et al. ⁶²	https://nbisweden.github.io/MrBayes/
MUSCLE v. 3.8	Edgar ⁶³	https://github.com/rcedgar/muscle
MAFFT v. 7.505	Katoh and Standley ⁶⁴	https://mafft.cbrc.jp/alignment/software/
IQ-TREE v. 2.0.3	Minh et al. ⁶⁵	http://www.iqtree.org/
TreeAnnotator v. 2.6.3	Bouckaert et al. ⁶⁶	https://beast.community/programs
R v. 4.2.2	R Core Team ⁶⁷	https://cran.r-project.org/
phytools v. 1.0-3	Revell ⁶⁸	https://github.com/liamrevell/phytools

RESOURCE AVAILABILITY

Lead contact

Further information and requests for resources and reagents should be directed to and will be fulfilled by the lead contact, Derek E.G. Briggs (derek.briggs@yale.edu).

Materials availability

The specimens are held by the Invertebrate Paleontology Division of the Yale Peabody Museum, New Haven, Connecticut, 06520, USA.

Data and code availability

A nexus file, including morphological, molecular, and stratigraphic information, as well as all parameters used for total-evidence phylogenetic inference, is available as Data S2.

EXPERIMENTAL MODEL AND SUBJECT DETAILS

The material comes from the late Silurian (Pridoli) Bertie Group (Bed A of the Williamsville Formation) in Ridgemount Quarry South, Fort Erie, Welland County, Ontario, Canada. See main text for further details.

METHOD DETAILS

Imaging and chemical analyses

Specimens were photographed with a Canon EOS 60D camera and EFS 60 mm lens, and close ups with a Canon EOS 5DSR camera and NP-E 65 mm lens. Specimens were imaged and analysed using a Hitachi SU7000 Scanning Electron microscope (SEM). Elemental analyses were carried out with an Energy Dispersive X-ray spectrometer (EDS) made by Oxford Instruments (Utilm Max-100 EDS system). The SEM was operated at acceleration voltage 15KV at variable pressure mode at 50 Pascals. Unfortunately, the density contrast between tube walls and matrix is insufficient to allow detection by CT scanning and serial sectioning was not considered an appropriate option given the small number of specimens available. Raman spectra were obtained using a Horiba LabRAM HR800 (532 nm, 20 mW, 1800 grooves/mm grating, 10 s acquisition time, 10 technical replicates mean averaged, 500 to





2000 cm-1) and processed in LabSpec 5 software. Spectra were despiked, baselined, smoothed, and analyzed in SpectraGryph 1.2. Individual Raman bands were identified from the spectra through an automated peak search.

QUANTIFICATION AND STATISTICAL ANALYSIS

Phylogenetic analyses

Rotaciurca superbus was incorporated into the most recent morphological dataset of fossil and extant hemichordates (Data S1 and S2).^{29,31} Stratigraphic ranges for all fossil terminals were compiled from the literature (Table S1). A few coding errors were corrected (Table S2), and contingent characters previously scored were changed to inapplicables, as these might bias the placement of *R. superbus*. The final morphological matrix was composed of 34 characters coded for 24 taxa, including the Cambrian stem-group enteropneusts *Oesia* and *Spartobranchus* as outgroups.⁸ *Gyaltsenglossus senis*, previously considered either a stem-group hemichordate⁸ or a stem-group pterobranch,⁶⁹ was also incorporated into the matrix.

Phylogenetic inference was performed under equal-weights parsimony using TNT v. 1.5^{61} and under Bayesian inference using MrBayes v. $3.2.7.^{62}$ For the former, an exhaustive search resulted in two optimal topologies, and support for nodes in the strict consensus was evaluated using 1,000 bootstrap replicates. For the latter, a variety of undated and tip-dated inferences were explored using the Mk_{pars} + Γ model of morphological evolution. To Tip dating used the fossilized birth-death (FBD) tree prior, fixing the extant sampling probability to the true value (determined using WoRMS), and using uninformative priors for remaining parameters (flat beta distribution for extinction and fossilization probabilities, exponential distribution with rate of 10 for speciation probability). A relaxed morphological clock assuming uncorrelated rate variation across branches (IGR) was implemented. A normal prior was set for the base clock rate (mean = 0.001, standard deviation = 0.01) and an exponential prior was used for the variance of the gamma distribution from which branch lengths are drawn (rate = 10). Stratigraphic ranges for tips were used as uniform age priors. Outgroup (enteropneust) and ingroup (pterobranch) monophylies were enforced, and a partial constraint was used for the split between *Cephalodiscus* and Graptolithina, leaving the position of *Rotaciurca* to resolve within either group, or as sister to both. Similarly, *Gyaltsenglossus* was free to resolve as a stem-group hemichordate, pterobranch, or enteropneust. Our results support the latter placements (Figure 4), unlike previous estimates. 8,69

Constraining the age of major hemichordate lineages is complicated by their poor preservation, paucity of diagnostic traits, sparse record in the early to middle Cambrian, and lack of precise dates for many relevant faunas. ^{6,31,39} Given this, we implemented conservative minimum and soft maximum dates through broad offset exponential prior distributions. Crown-group Hemichordata was constrained to be older than 529.0 Ma (base of Cambrian Stage 2) based on records of the pterobranch *Sokoloviina costata* from the Lontova Formation in Estonia. ⁷³ A mean of 546.24 was used, as this value results in 95% of the prior probability to reside between the minimum bound and 580 Ma, which matches previous estimates for the age of crown-group Ambulacraria. ⁷⁴ Therefore, this prior (applied to the age of the tree) spans the entire range of possible times of origin of crown hemichordates from their stem group, and places high probability close to even older plausible records of *S. costata* in the early Cambrian (Fortunian) Rovno Horizon in Ukraine. ⁶ Pterobranch origins were constrained with a minimum age of 514.0 Ma (base of Cambrian Stage 4) given the many colonial pterobranchs recorded around this time, representing the oldest definitive members of Graptolithina. ⁶ The mean of the distribution was set to 522.28 Ma, generating a 95% prior distribution that extended to the base of the Cambrian.

Rooting is a problem for inferring pterobranch relationships given lack of suitable morphological outgroups.²⁹ While a recent analysis rooted trees using tubicolous stem-group enteropneusts,³¹ calibrated inference can root trees using the node inferred to be oldest in the absence of explicit outgroups. Tip dating can also accommodate changes in the overall tree structure through time, which is relevant given the heterogeneity of the hemichordate fossil record. Inference was therefore performed with and without outgroups, as well as with constant-rate and skyline FBD models⁷⁵ (with an epoch transition at the end of the Carboniferous, by which time all non-Rhabdopleura graptolites were certainly extinct).^{76,77} Neither rooting nor tree prior modified the overall results (Figures S3C–S3F), and confirm recent insights on the relationships among fossil and extant hemichordates under a much expanded set of inference conditions.

Finally, total-evidence inference was performed after adding data for 13 mitochondrial protein coding loci (PCLs; coded as amino acids) and the 18S ribosomal DNA (coded as nucleotides). PCLs were obtained from the mitogenomes of *Saccoglossus kowalevskii*, *Rhabdopleura compacta*, and *Cephalodiscus* (C.) *hodgsoni*, ⁴⁶ and aligned with MUSCLE v. 3.8⁶³ under default settings. The rDNA dataset included the same taxa, as well as *C.* (*Orthoecus*) *densus* and *C. planitectus* (which is the sister group to all other extant members of the genus, defining their crown group), ⁴⁷ and was aligned with the L-INS-I method in MAFFT v. 7.505. ⁶⁴ For all alignments, positions with over 50% gaps were manually trimmed. Optimal models were obtained with IQ-TREE v. 2.0.3 ⁶⁵; in the case of the PCLs merging loci into three partitions. ^{78,79} Separate uncorrelated clocks were used for each of the three data types (morphology, nucleotides, and amino acids).

Four runs of four chains each were continued for 50 (undated), 80 (tip-dated, morphology only) and 100 (tip-dated, total evidence) million generations, and the initial 50% was discarded as burn-in. Runs under a constant-rate FBD model (Figures S3C and S3D) did not converge, and are shown only for illustrative purposes. For uncalibrated (Figure S3B) and tip-dated skyline analyses (using morphological and total-evidence datasets; Figures S3E and S4, respectively), average effective sample sizes of parameters were larger than 356.1, and potential scale reduction factors were less than 1.017.

Divergence times for crown-group hemichordates and pterobranchs were compared with those obtained under the joint prior (shown in Figure 4, inset).⁸⁰ Dates under the joint prior were obtained under the same analytical conditions used to generate Figure 4,



yet without employing the morphological and molecular datasets. This confirmed that prior dates contained older estimates than those inferred under morphological or total-evidence dating. Dates as old as 644.9 Ma and 596.7 Ma were sampled under the joint prior for hemichordates and pterobranchs, respectively. While total-evidence dating discarded old origination dates of high prior probability, resulting in 95% confidence intervals with truncated upper ends, dating under the morphological clock resulted in a shift of 95% confidence intervals towards older origination times (Figure 4).

Ancestral state reconstructions

The evolutionary history of life-style (solitary/pseudocolonial/colonial), ecology (planktic/benthic), and tube-building (present/absent) was assessed using 1,000 replicates of stochastic character mapping⁸¹ under equal-rate models. Analyses relied on a maximum clade credibility (mcc) tree obtained from the posterior sample of topologies with TreeAnnotator v. 2.6.3,66 and were run in the R statistical environment v. 4.2.267 using function make.simmap from package phytools.68

Current Biology, Volume 33

Supplemental Information

A Silurian pseudocolonial pterobranch

Derek E.G. Briggs and Nicolás Mongiardino Koch

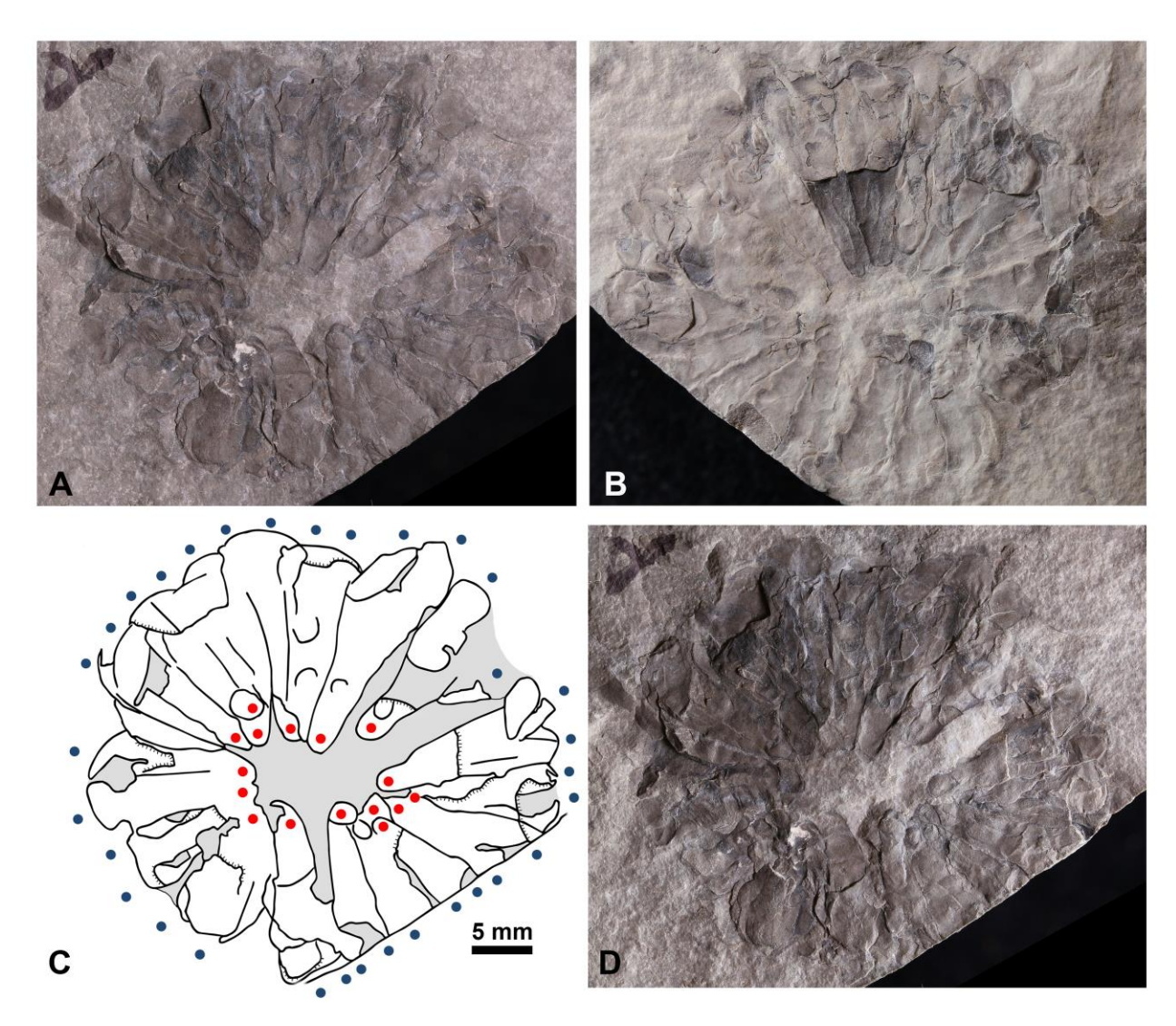


Figure S1. *Rotaciurca superbus* sp. nov. YPM IP 546797, related to Figures 1, 2. (A,B) part and counterpart, high angle illumination. (C,D) part and explanatory drawing, low angle illumination. Red dots mark the origins (closed ends) of tubes where evident on part or counterpart, blue dots represent the termination of tubes.

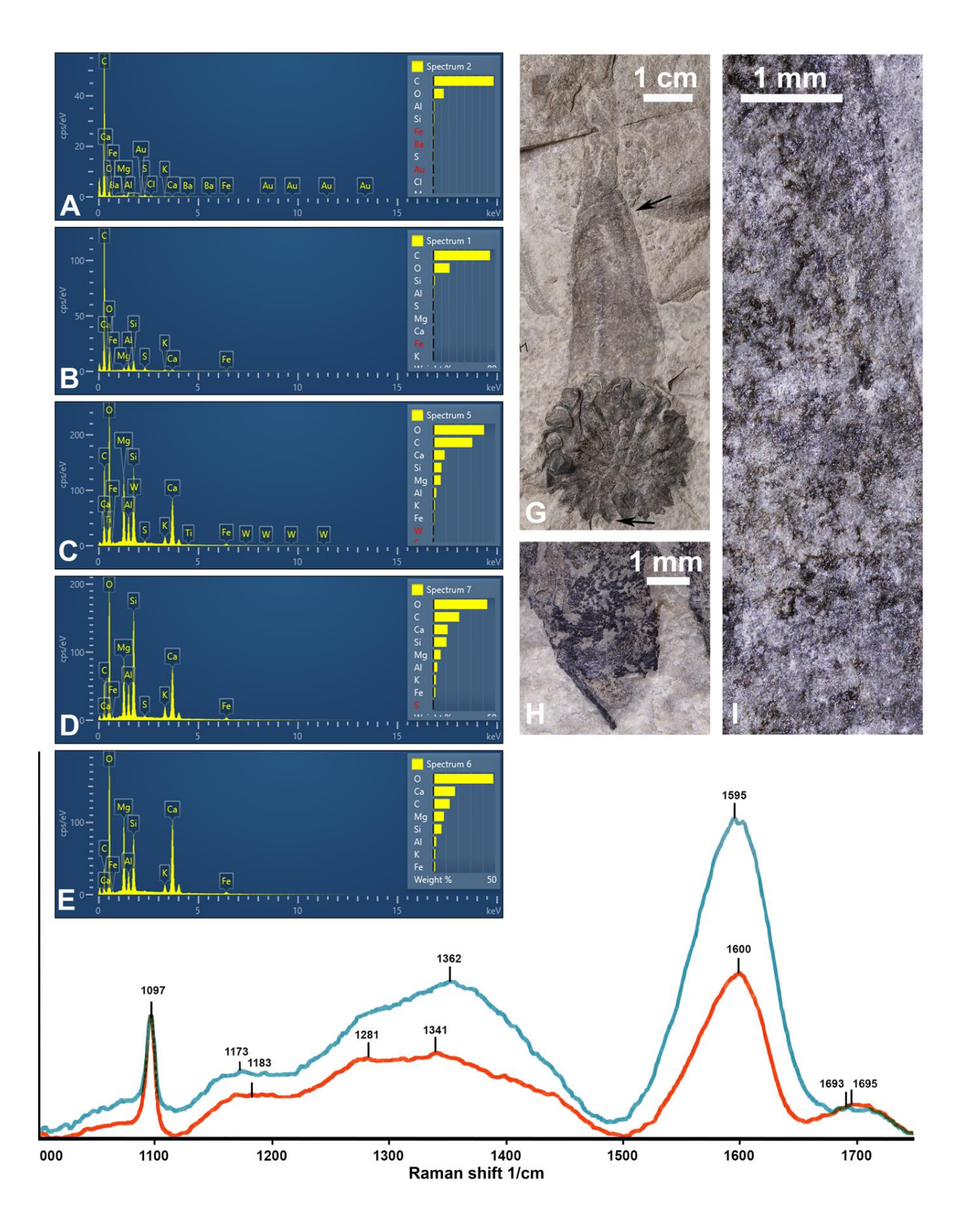


Figure S2. Evidence of the composition of the skeleton of *Rotaciurca superbus*, related to Figure 3. (A-E) EDS data on *Rotaciurca superbus* samples. (A) YPM IP 428141 (illustrated in G) fusellum. The source of the sample (extracted and mounted on an SEM stub) is indicated as s in Figure 1I. Note the dominance of C. (B) YPM IP 428141, associated eurypterid tergite. The sample (extracted and mounted on an SEM stub) is from an isolated tergite 13.4 cm from the edge of the tubarium on the part (Figure 1A). Note the dominance of C. (C) YPM IP 237272 (Figure 2D,E), fusellum of tube indicated fus in Figure 2E (images in Figure 3E,F). The entire specimen was analysed in the environmental chamber of the SEM. (D) YPM IP 237272 (Figure 2D,E), dark featureless area in the center of the tubarium. Note lower C peak and high Si peak relative to (C). (E) YPM IP 237272 (Figure 2D,E), sediment adjacent to the tubarium. Note lower C peak relative to (D). The horizontal Weight % divisions each represent 10 percentage points. (F) YPM IP 428141 (illustrated in G) Raman spectrum (blue) of area of tube in (H), compared to that of cuticle from the eurypterid fragment (red) from the same sample for comparison. (G-I) YPM IP 428141. (H,I) Close-ups of tube and area of conical structure showing dark colored fragments of wall. Positions indicated by arrows in (G).

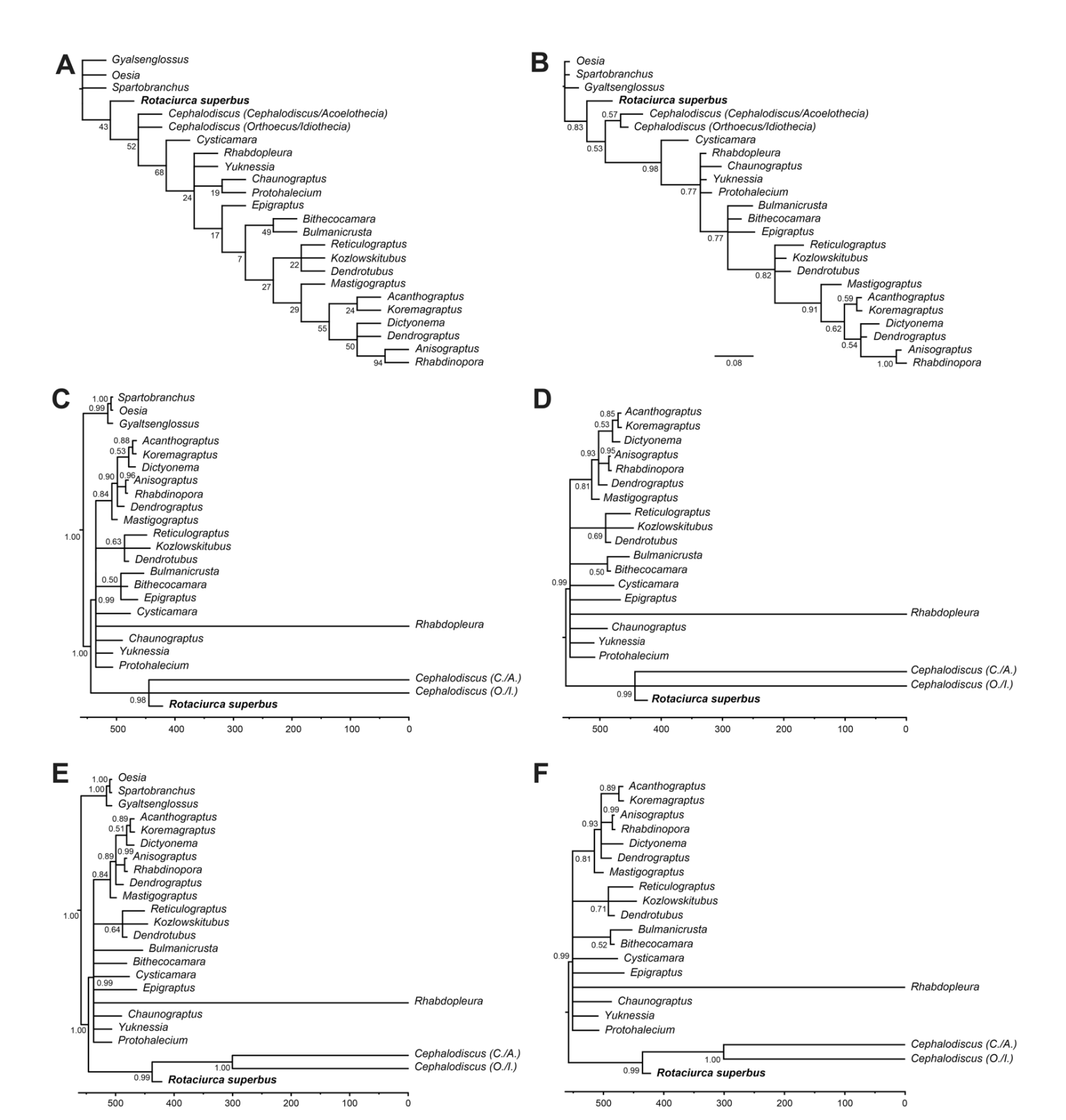


Figure S3. Morphological phylogenies exploring the placement of *Rotaciurca* **among hemichordates, related to Figure 4.** (A) Strict consensus of two most-parsimonious topologies, with support values estimated using 1,000 replicates of bootstrap resampling. (B) Bayesian majority-rule consensus, with support values estimated as posterior probabilities. (C) Constant-rate FBD analysis rooted using enteropneus outgroups. (D) Constant-rate FBD analysis rooted on the node inferred to be oldest (i.e., without outgroups). (E) Skyline FBD analysis rooted using enteropneust outgroups. (F) Skyline FBD analysis rooted on the node inferred to be oldest (i.e., without outgroups). Phylogenies C-F represent majority rule consensus trees, and node values are posterior probabilities. Axes represent geological time in millions of years. Skyline FBD analyses implemented a shift in speciation, extinction, and fossilization probabilities at the end of the Carboniferous (298.9 Ma). Analyses under constant-rate FBD models (C-D) did not converge and are shown only for illustrative purposes. Analytical conditions used to infer the tree in (E) are the ones also used for total-evidence dating.

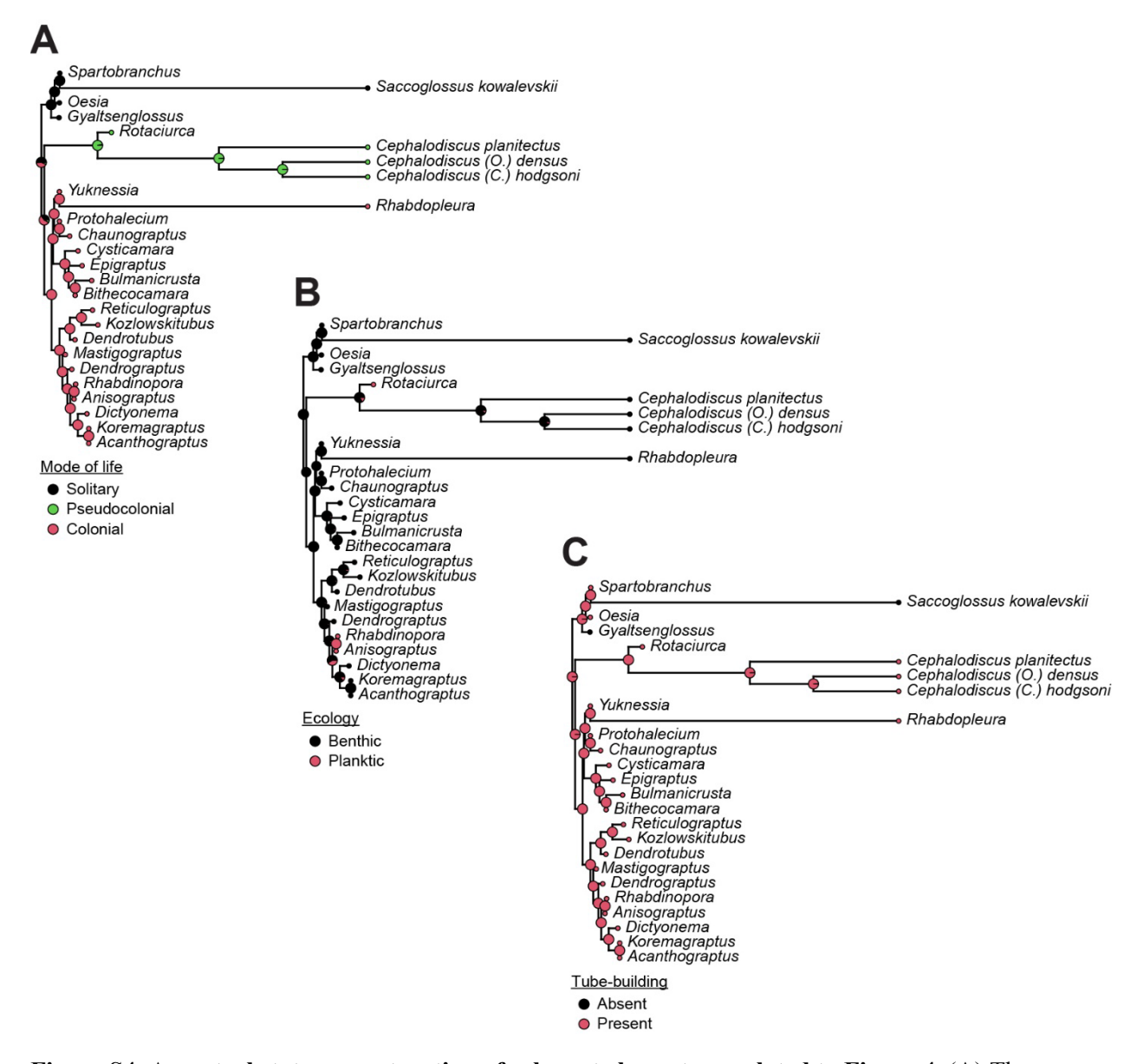


Figure S4. Ancestral state reconstruction of relevant characters, related to Figure 4. (A) The evolution of hemichordate mode of life, and the origin of coloniality in the clade, remain ambiguous. (B) A planktic lifestyle evolved independently in graptoloids and *Rotaciurca*. (C) Tube-dwelling is inferred to be ancestral for hemichordates.

Taxon	Stratigraphic age	Tip dates (notes)	Reference					
Acanthograptus	?Cambrian (Miaolingian, Drumian,	~504.5 – 425.6 (down to age,	Maletz ^{S1}					
	Goniagnostus nathorsti Biozone)-Silurian,	not biozone, but the						
	Ludlow (Gorstian, Saetograptus chimaera	Drumian is only 4 my long						
	Biozone)	and the Gorstian 2 my)						
Koremagraptus	?Cambrian (Furongian)–Lower Devonian (Lochkovian)	~497 – 410.8	Maletz ^{S1}					
Anisograptus	Lower Ordovician (lower Tremadocian,	485.4 – 477.7 (= range for	Maletz et al. ^{S2}					
	Anisograptus matanensis–Rhabdinopora	entire Tremadocian but						
	flabelliformis anglica Biozones)	lower Tremadocian would						
		end around 481.5 assuming						
		it's half the length)						
Rhabdinopora	Lower Ordovician (lower Tremadocian,	485.4 – 477.7 (same as for	Maletz et al. ^{S2}					
	Rhabdinopora flabelliformis praeparabola–	Anisograptus)						
	Adelograptus Biozones)							
Dictyonema	Cambrian (Miaolingian)—?Carboniferous	~509 – ?298.9	Maletz ^{S1}					
Dendrograptus	Furongian (Jiangshanian)-?Devonian	~494 – ?358.9	Maletz ^{S1}					
Mastigograptus	Cambrian, Maolingian, Wuliuan to Upper	509 – 445.2	Ramírez-Guerrero and					
	Ordovician (Sandbian–Katian)		Cameron ^{S3} ; Maletz ^{S2}					
Reticulograptus	Lower Ordovician (Tremadocian)–Silurian (Wenlock):	485.4 – 427.4	Maletz ^{S2}					
Kozlowskitubus	Upper Ordovician (Katian)–Silurian (Ludlow)	453.0 – 423.0	Maletz ^{S4}					
Dendrotubus	Lower Ordovician (Tremadocian)	485.4 – 477.7	Maletz ^{S4}					
Bulmanicrusta	Middle Ordovician (Darriwilian)–Upper Silurian (Ludlow)	467.3 – 423.0	Maletz ^{S4}					
Bithecocamara	Lower Ordovician (Tremadocian)	485.4 – 477.7	Maletz ^{S4}					
Cysticamara	Lower Ordovician (Tremadocian)–Middle Ordovician (Darriwilian)	485.4 – 458.4	Maletz ^{S4}					
Epigraptus	Lower Ordovician (Tremadocian)–Upper Ordovician	485.4 – 443.8	Maletz and Beli ^{SS}					
Chaunograptus	Cambrian (Maolingian, Wuliuan,	509 – 427.4	Maletz and Beli ^{S5}					
<i>5</i> ,	Ptychagnostus praecurrens Biozone)–Silurian							
	(Wenlock)							
Yuknessia	Cambrian (Maolingian, Wuliuan,	509 – 504.5	LoDuca et al. ^{S6}					
	Bathyuriscus/Elrathina–Ptychagnostus							
	punctuosus Biozone)							
Spartobranchus	Cambrian, Maolingian, Wuliuan, Burgess Shale	509 – 504.5	Caron et al. ^{S7}					
Oesia	Cambrian, Maolingian, Wuliuan, Burgess Shale	509 – 504.5	Nanglu et al. ^{S8}					
Gyaltsenglossus	Cambrian, Maolingian, Wuliuan, Burgess Shale	509 – 504.5	Nanglu et al. ^{S8}					
Protohalecium	Cambrian, Maolingian, Wuliuan	509 – 504.5	Ramírez-Guerrero and					
	· , · · · · · · · · · · · · · · · · · ·		Cameron ^{S3}					
Rotaciurca	Bertie Group, Ontario, Canada, Silurian, Pridoli	423 – 419.2	This study					

Table S1. Stratigraphic ranges of terminals included in the matrix, related to Figure 4 and Data S2.

Although extant genera (*Cephalodiscus*, *Rhabdopleura*) have extensive fossil records in the Paleozoic, their tip ages were constrained to the present when the molecular data for them is observed. Dates are taken from the International Chronostratigraphic Chart v. 2022/10.^{S9}

Oesia	0	-	-	0	0	0	-	-	-	-	0	0	0	0	0	0	0	0	0	1	0	1	0	0	0	0	0	0	0	0	0	0	1	0
Spartobranchus	0	-	-	0	0	0	-	-	-	-	0	0	0	0	0	0	0	0	0	1	0	1	0	0	0	0	0	0	0	0	0	0	0	0
Acanthograptus	2/3	3?	2	?	0	1	?	1	2	1	2	1	4	0	1	0	1	1	0	2	0	1	2	?	0	0	0	1	0	2	3	1	0	1
Koremagraptus	?	?	?	?	0	1	?	1	2	?	2	1	4	0	1	0	1	1	0	2	0	1	2	?	0	0	0	1	0	2	3	?	0	1
Anisograptus	3	1	2	2	0	1	1	3	2	0	2	1	4	0	1	1	1	0	1	2	0	2	1	2	0	0	0	1	0	2	3	1	0	1
Rhabdinopora	3	1	2	2	0	1	1	3	2	0	2	1	4	0	1	1	1	2	1	2	0	2	1	2	0	0	0	1	0	2	3	1	0	1
Dictyonema	2/3	3?	2	?	0	1	1	1	2	1	2	1	4	0	1	0	1	3	1	2	0	2	2	?	0	0	0	1	0	2	3	1	0	1
Dendrograptus	2	1	2	2	0	1	1	1	2	1	2	1	4	0	1	0	1	0	0	2	0	2	1	2	0	0	0	1	0	2	3	?	0	1
Mastigograptus	2	?	2	?	0	1	?	1	2	1	2	1	4	0	1	0	0	0	0	1	0	1	1	1	0	0	0	1	0	2	3	1	0	1
Reticulograptus	?	?	?	?	?	1	?	1	2	?	1	1	?	0	1	0	0	1	1	1	0	1	2	2	0	0	1	1	0	?	?	?	0	1
Kozlowskitubus	1	1	2	1	1	1	1	1	1/2	1	1	1	1	1	1	0	0	2	0	1	0	1	2	2	0	0	0	1	0	2	3	0	0	1
Dendrotubus	1	1	2	1	1	1	1	1	2	1	1	1	3	1	1	0	0	1	0	1	0	1	2	2	1	0	0	1	1	?	?	?	0	1
Bulmanicrusta	1	0	2	2	?	1	0	2	1	1	2	1	1	1	0	0	0	0	0	1	1	1	0	2	0	2	0	1	0	1/2	2 2/3	3 0	0	1
Bithecocamara	?	?	?	?	?	1	?	1	2	1	2	1	2	1	0	0	0	0	0	1	1	1	0	2	0	0	0	1	0	?	?	?	0	1
Cysticamara	?	?	?	?	?	1	?	1	3	1	1	0	0	1	0	0	0	0	0	1	1	1	0	2	0	0	0	0	1	?	?	?	0	1
Epigraptus	1	0	1	2	1	1	0	1	2	?	2	1	3	1	0	0	0	0	0	1	0	1	0	2	0	0	1	1	1	?	?	0	0	1
Rhabdopleura	1	0	1	2	1	1	0	1	2	1	1	1	1	1	0	0	0	0	0	1	0	1	0	1	0	1	0	0	0	2	0	0	0	1
Chaunograptus	?	?	?	?	?	1	?	?	?	?	1	1	?	?	0	0	0	0	1	1	0	1	1	?	0	0	0	0	?	?	?	?	0	1
Yuknessia	?	?	1	?	?	1	?	?	?	?	1	1	?	1	0	0	0	0	0	1	0	1	0	1	0	0	0	0	?	?	?	?	0	1
Protohalecium	?	?	?	?	?	?	?	?	?	?	?	?	?	1	?	0	?	0	0	1	0	1	1	1	0	0	0	?	?	?	?	?	0	1
Cephalodiscus (C./A.)	0	-	-	0	0	0	-	-	-	-	0	0	0	1	0	0	0	0	0	0	0	0	0	1	0	0	0	0	1	?	?	?	0	2
Cephalodiscus (O./I.)	0	-	-	0	0	0	-	-	-	-	0	0	0	1	0	0	0	0	0	1	0	1	0	1	0	0	0	0	1	0	1	0	0	2
Rotaciurca	0	-	-	0	0	0	-	-	-	-	0	0	0	0	0	1	0	0	1	1	0	1	0	1	0	0	0	0	0	?	?	?	0	2
Gyaltsenglossus	0	-	-	0	0	0	-	-	-	-	0	0	0	0	0	0	0	0	0	0	-	-	-	-	-	0	0	0	0	-	0	0	0	0

Table S2. Morphological data matrix, related to Figure 4, Data S1 and Data S2. Based on Ramírez-Guerrero and Cameron, S3 with revised character codings as explained in Data S1, and with the addition of *Rotaciurca superbus* and *Gyaltsenglossus senis*. Note that the datafile used for total-evidence, tip-dated inference under a skyline FBD model (and including the morphological and molecular datasets) is provided as Data S2.

Supplemental references

- S1. Maletz, J. (2020). Part V, Second revision, Chapter 17: Order Dendroidea: Introduction, morphology, and systematic descriptions. Treatise Online 100, 1-8.
- S2. Maletz, J., Toro, B.A., and Zhang, Y. (2017). Part V, Second revision, Chapter 18: Order Graptoloidea and Family Anisograptidae: Introduction, morphology, and systematic descriptions. Treatise Online 85, 1-14.
- S3. Ramírez-Guerrero, G.M., and Cameron, C.B. (2021). Systematics of pterobranchs from the Cambrian Period Burgess Shales of Canada and the early evolution of graptolites. Bull. Geosci. 96, 1-18.
- S4. Maletz, J. (2019). Part V, Second revision, Chapter 16: Order Graptolothina, uncertain families: Introduction, morphology, and systematic descriptions. Treatise Online 122, 1-19.
- S5. Maletz, J., and Beli, E. (2018). Part V, Second Revision, Chapter 15: Subclass Graptolithina and Incertae Sedis Family Rhabdopleuridae: Introduction and systematic descriptions. Treatise Online 101, 1-14.
- S6. LoDuca, S.T., Caron, J.-B., Schiffbauer, J.D., Xiao, S., and Kramer, A. (2015). A reexamination of Yuknessia from the Cambrian of British Columbia and Utah. J. Paleont. 89, 82-95.
- S7. Caron, J.-B., Conway Morris, S., and Cameron, C.B. (2013). Tubicolous enteropneusts from the Cambrian period. Nature 495, 503–506.
- S8. Nanglu, K., Caron, J.-B., Conway Morris, S., and Cameron, C.B. (2016). Cambrian suspension-feeding tubicolous hemichordates. BMC Biol. 14, 56.
- S9. Cohen, K.M., Finney, S.C., Gibbard, P.L., and Fan, J.-X. (2013). The ICS International Chronostratigraphic Chart. Episodes 36, 199-204. Updated http://www.stratigraphy.org/ICSchart/ChronostratChart2022-10.pdf
- S10. Mitchell, C.E., Melchin, M.J., Cameron, C.B., and Maletz, J. (2013). Phylogenetic analysis reveals that Rhabdopleura is an extant graptolite. Lethaia 46, 34-56.
- S11. Bulman, O.M.B. (1970). Part V: Graptolithina with sections on Enteropneusta and Pterobranchia. Treatise on Invertebrate Paleontology. 163 pp. The Geological Society of America and the University of Kansas, US.
- S12. Kozlowski, R. 1949. Les graptolithes et quelques nouveaux groupes d'animaux du Tremadoc de la Pologne. Acta Palaeontol. Pol. 3, 1-330.
- S13. Maletz, J. (2019). *Dictyonema* Hall and its importance for the evolutionary history of the Graptoloidea. Palaeontology 62, 151-161.
- S14. Urbanek, A. (1983). The significance of graptoblasts in the life cycle of crustoid graptolites. Acta Palaeontol. Pol. 28, 313-326.

- S15. Urbanek, A., and Mierzejewski, P. (1984). The ultrastructure of the Crustoidea and the evolution of graptolite skeletal tissues. Lethaia 17, 73-91.
- S16. Urbanek, A., and Towe, K.M. (1974). Ultrastructural studies on Graptolites 1. The Periderm and its derivatives in the Dendroidea and in Mastigograptus. Smithson. Contrib. Paleobiol. 20, 1-49.
- S17. Landing, E., Antcliffe, J.B., Geyer, G., Kouchinsky, A., Bowser, S.S. and Andreas, A. (2018). Early evolution of colonial animals (Ediacaran Evolutionary Radiation—Cambrian Evolutionary Radiation—Great Ordovician Biodiversification Interval). Earth Science Reviews 178, 105-135.